nature geoscience

ARTICLES

https://doi.org/10.1038/s41561-018-0268-4

Nutrient release to oceans from buoyancy-driven upwelling at Greenland tidewater glaciers

Mattias R. Cape[1,2*], Fiammetta Straneo[1,3], Nicholas Beaird[1,4], Randelle M. Bundy[2,5] and Matthew A. Charette[5]

The discharge of nutrient-rich meltwater from the Greenland Ice Sheet has emerged as a potentially important contributor to regional marine primary production and nutrient cycling. While significant, this direct nutrient input by the ice sheet may be secondary to the upwelling of deep-ocean-sourced nutrients driven by the release of meltwater at depth in glacial fjords. Here, we present a comprehensive suite of micro- and macronutrient observations collected in Sermilik Fjord at the margin of Helheim, one of Greenland's largest glaciers, and quantitatively decompose glacial and ocean contributions to fjord dissolved nutrient inventories. We show that the substantial enrichment in nitrate, phosphate and silicate observed in the upper 250 m of the glacial fjord is the result of upwelling of warm subtropical waters present at depth throughout the fjord. These nutrient-enriched fjord waters are subsequently exported subsurface to the continental shelf. The upwelled nutrient transport within Sermilik rivals exports by the largest Arctic rivers and the ice sheet as a whole, suggesting that glacier-induced pumping of deep nutrients may constitute a major source of macronutrients to the surrounding coastal ocean. The importance of this mechanism is likely to grow given projected increases in surface melt of the ice sheet.

Dramatic changes in land ice at both poles, as a result of sustained warming of both the atmosphere and ocean, have brought into focus the significant role of ice sheets and glaciers in mediating marine ecosystem processes in polar and subpolar oceans[1,2]. While the impact of increased freshwater export from the Greenland Ice Sheet (GrIS) on the physical environment is now appreciated[3], recent studies have uncovered that some meltwater is also rich in nutrients (for example, silica, iron) as a result of biogeochemical cycling and weathering at the ice sheet surface, interior and bed[4–10]. These observations have led to the hypothesis that the summer-enhanced discharge of nutrient-rich meltwater into Greenland's coastal waters[6], particularly along the East Greenland coast[11], may play an important role in sustaining primary production downstream in the North Atlantic Ocean at a time when marine ecosystems are nutrient and potentially light limited[8,12,13]. Projected increases in Greenland melt could then drive an increase in nutrient export to the coastal ocean, with repercussions for biogeochemical cycling downstream.

Recent observations collected at the marine margins of glaciers, however, suggest that meltwater may not be the sole nutrient contributor along Greenland margins[14,15]. For Greenland's marine-terminating glaciers[16,17], which drain an estimated 88% of the ice sheet and have significantly contributed to the recent anomalous mass loss[18,19], a substantial fraction of the meltwater is released hundreds of metres below the ocean surface as subglacial discharge (SGD; surface runoff routed to the ice-sheet bed and exported at the base of the glaciers) and submarine meltwater (SMW; subsurface melt of glacial ice by the ocean)[20]. Calved icebergs also contribute significantly to SMW export as a result of melting during transit from the glacier margin to the open ocean[21]. These inputs of buoyant freshwater at depth drive vigorous upwelling of deep ocean waters towards the sunlit ocean surface at the glacial margin[17,22,23], resulting in the formation of glacially modified water (GMW), a new water mass that contains both deep, ambient water masses and glacial sources[24,25]. GMW formed in this manner has previously been observed in Greenland glacial fjords as thick layers spanning the top 100–200 m of the water column[24–28]. This suggests that previous observations of nutrient enhancement of coastal waters may, in part, be due to a neglected source—the buoyancy-driven upwelling of nutrient-rich deep waters at the glacial margins[14,15]. Biogeochemical observations to quantify the relative contribution of nutrients from upwelling versus those contained only in meltwater (that is, SMW + SGD) have been unavailable until recently. In light of the observed and projected increase in ice loss from Greenland[29], constraining the role of the ice sheet and deep ocean waters as nutrient sources to the upper water column is critical to our ability to project future marine ecosystem changes in the subpolar North Atlantic[11,12].

Glacial water mass transformation

Here we investigate the nutrient sources within the GMW exported from Sermilik Fjord, Southeast Greenland, by analysing the biogeochemical and physical properties of waters in the fjord and on the shelf in a survey conducted in August 2015 (Fig. 1a). The narrow (~6 km), 100-km-long and 600–900-m-deep fjord links Helheim Glacier, Greenland's fifth largest outlet glacier by discharge grounded 600 m below sea level[16], to the Irminger Sea and the North Atlantic. Sermilik's deep sills (~500 m) allow for an unimpeded flow of shelf waters to the glacial margins. Discrete water samples were collected alongside continuous conservative temperature–absolute salinity (Θ–S_A) profiles at ten hydrographic stations inside and five outside the fjord for analysis of water column dissolved macronutrients (nitrate: NO_3^-; silicate: $Si(OH)_4$; phosphate: PO_4^{3-}) and surface total dissolvable iron (TdFe; comprising dissolved and labile particulate iron) (Fig. 1a). Given the east to west flow of the current

[1]Department of Physical Oceanography, Woods Hole Oceanographic Institution, Woods Hole, MA, USA. [2]School of Oceanography, University of Washington, Seattle, WA, USA. [3]Climate, Atmospheric Sciences, and Physical Oceanography Department, Scripps Institution of Oceanography, University of California, San Diego, La Jolla, CA, USA. [4]College of Earth, Ocean, and Atmospheric Sciences, Oregon State University, Corvallis, OR, USA. [5]Department of Marine Chemistry and Geochemistry, Woods Hole Oceanographic Institution, Woods Hole, MA, USA. *e-mail: mcape@uw.edu

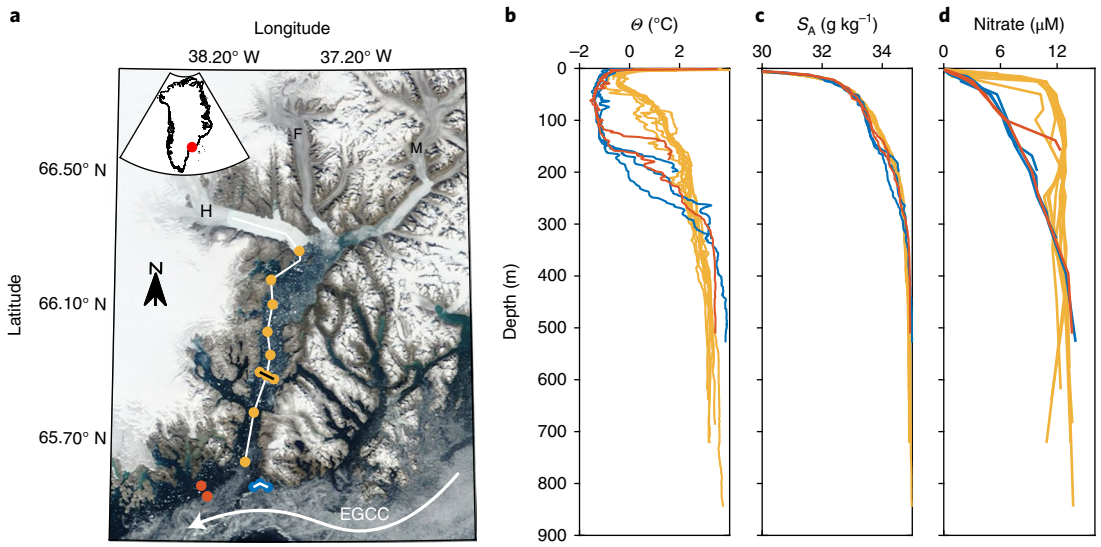

Fig. 1 | Sermilik Fjord study region and hydrography in August 2015. a, MODIS (Moderate Resolution Imaging Spectroradiometer) Terra image of Sermilik Fjord collected on 9 August 2015 during the sampling period, showing the position of occupied stations. Note the presence of sea ice along the continental shelf outside of Sermilik at the time of sampling. Stations are coloured by location for reference in **b**–**d** as well as Fig. 3a: stations upstream from the fjord (blue), within the fjord (yellow) and downstream (red). The white lines inside the fjord and upstream indicates the along-fjord and shelf sections shown in Fig. 2 and Supplementary Fig. 8, while the black line mid-fjord corresponds to the cross-shelf section used for fjord export calculations (Supplementary Fig. 6). The white arrow outside of Sermilik indicates the path of the East Greenland Coastal Current (EGCC). Locations of glaciers terminating in Sermilik are indicated by H (Helheim), F (Fenris) and M (Midgaard). The inset map indicates the general location of Sermilik Fjord. **b**–**d**, Profiles of conservative temperature, Θ (**b**), absolute salinity, S_A (**c**) and nitrate concentrations (**d**) for stations indicated in **a**.

across the mouth of the fjord[30,31], stations to the east of the fjord are representative of continental shelf waters (that is, are upstream of any glacier-induced modification within Sermilik[32]), while stations to the west lie downstream of the fjord[26].

Source waters entering the fjord from the continental shelf are initially well stratified, with a layer of cold Polar Water (PW) of Arctic origin in the top 200 m (with endmember properties $\Theta = -1.40$ °C, $S_A = 33.41$ g kg^{-1}), separated by a sharp pycnocline from Atlantic Water (AW) of subtropical origin below ($\Theta = 3.21$ °C, $S_A = 34.89$ g kg^{-1}) (Figs. 1b,c and 2a and Supplementary Fig. 1). In contrast, waters found in the top 250 m of the fjord have properties that are distinct from those identified on the shelf. While near-surface (<5 m) waters in this layer are warmer ($\Theta = 0.91 \pm 1.16$ °C) and fresher (22.00 ± 6.90 g kg^{-1}) than surface waters upstream of the fjord ($\Theta = -0.60 \pm 0.38$ °C, $S_A = 28.75 \pm 0.74$ g kg^{-1}), subsurface waters (<250 m) are warmer ($\Theta = 1.53 \pm 0.83$ °C) and saltier (33.96 ± 0.55 g kg^{-1}) than PW, yet colder and fresher than AW. Earlier studies have identified these waters as GMW[26,31–35]—a mixture of upwelled AW, PW and different meltwater sources—formed as a result of glacier, iceberg and ocean exchanges.

Observations of nutrient enrichment and transport

Differences in the physical characteristics of the fjord's upper water column are parallelled by a striking disparity in macronutrient load. Fjord waters in the upper 250 m are significantly enriched in macronutrients ($NO_3^- = 12.0 \pm 0.84$ μM, $Si(OH)_4 = 6.67 \pm 0.65$ μM, $PO_4^{3-} = 0.72 \pm 0.05$ μM) relative to waters found at similar depths on the continental shelf ($NO_3^- = 6.19 \pm 0.44$ μM, $Si(OH)_4 = 4.82 \pm 0.21$ μM, $PO_4^{3-} = 0.61 \pm 0.02$ μM; Figs. 1c and 2c,e,g and Supplementary Figs. 1 and 2), and instead have concentrations similar to those of deep (>300 m) shelf waters ($NO_3^- = 12.3 \pm 1.20$ μM, $Si(OH)_4 = 6.22 \pm 0.77$ μM, $PO_4^{3-} = 0.74 \pm 0.08$ μM). While macronutrients are drawn down in the euphotic zone (~30 m throughout the fjord), consistent with enhanced local (fjord-scale) primary and secondary productivity at tidewater glacier margins[14,15,36], silicate and TdFe concentrations remain elevated in surface waters <5 m in the fjord and, in the case of TdFe, downstream ($Si(OH)_4 = 3.46 \pm 1.64$ μM, TdFe = 6.96 ± 4.68 nM; Supplementary Fig. 3). Nutrient enrichment of this magnitude has previously been reported in the upper 100 m of other Greenland glacial fjord systems[10,14,15,37,38]. Biogeochemical modification within this major fjord are by comparison far more extensive, spanning the entire upper 250 m of the water column and the length of the 100-km-long fjord (Fig. 2).

To confirm that these nutrient-enriched waters are indeed GMW, we examine along-isopycnal property anomalies relative to upstream conditions (Fig. 2b,d,f,h), alongside Θ–S_A characteristics of the water masses (Fig. 3). In this framework, water mass modification as a result of interaction with the glacier (including SGD) would be characterized by anomalies that decay away from the glacial terminus[26], and Θ–S_A properties consistent with transformation of ambient water masses by addition of SGD and SMW[39,40] (Fig. 3a). Within the fjord, weak temperature and nutrient anomalies are apparent below 250 m (apart from phosphate, which shows strong negative anomalies associated with high turbidity at depth, see Supplementary Fig. 4) (Fig. 3d,f,h), with Θ–S_A properties in this layer resembling a mixture of AW and PW (that is, the ambient trend; Fig. 3a), suggesting that these waters are unmodified. Above 250 m, Θ–S_A properties instead fall between the ambient trend and the melt (that is, SMW) and runoff (that is, SGD) mixing lines[26,39,40], with nutrient and temperature anomalies consistent with the vertical redistribution of AW driven by mixing with SGD and SMW. In addition, these observations are also consistent with noble gas observations collected concurrently during the cruise[32], whose chemical signatures provide definitive evidence for the presence of SMW and SGD in the upper layer of the fjord.

Previous studies have shown that this upper layer (<250 m) is exported to the shelf by the mean summer circulation[35] (Supplementary Fig. 5). The vertical distribution and biogeochemical properties of GMW in the fjord show that summertime circulation will drive the export of nutrient-rich GMW to the continental

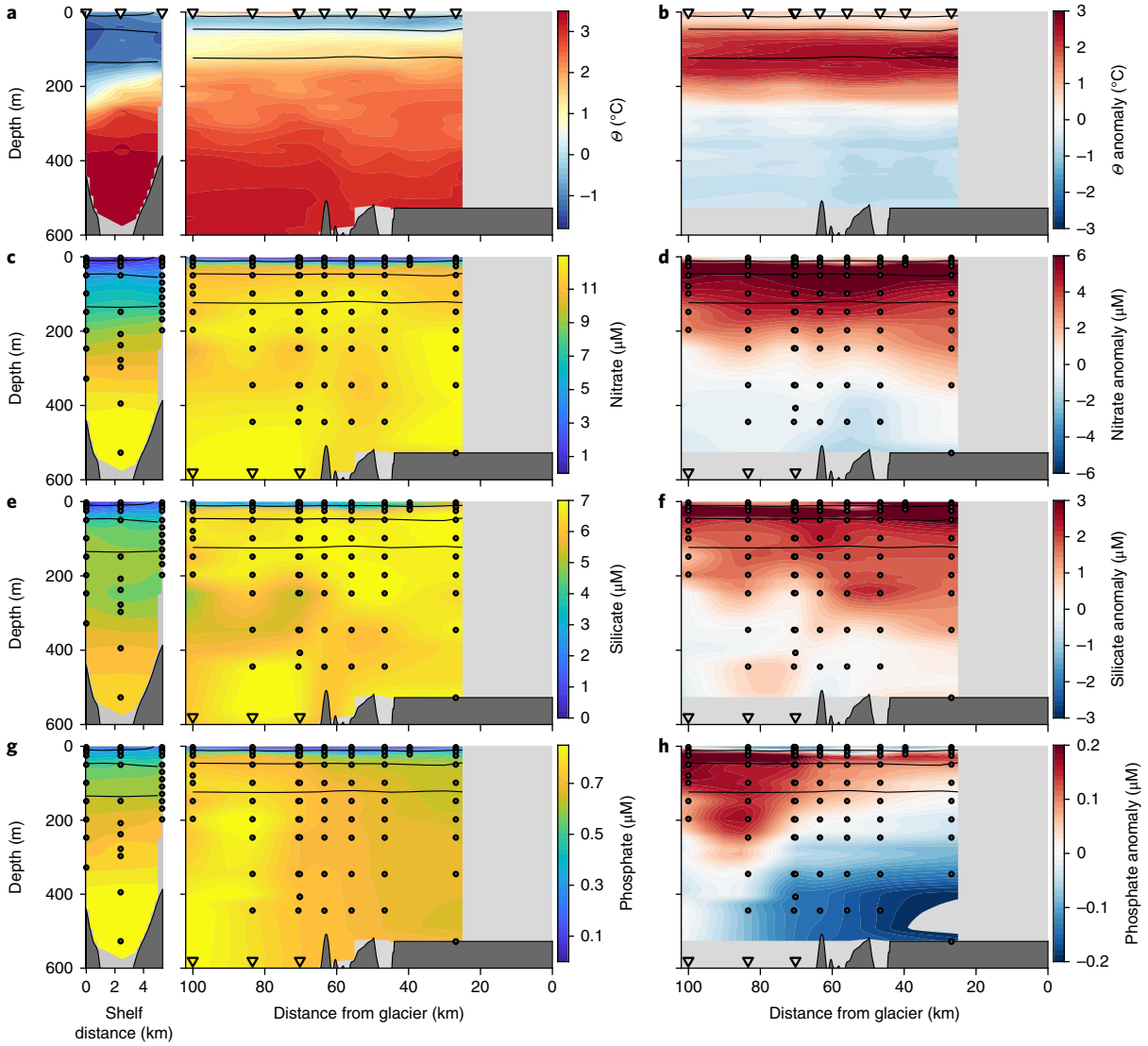

Fig. 2 | Shifts in upper water column physical and chemical properties resulting from glacially driven circulation. a,**c**,**e**,**g**, Along-fjord sections of conservative temperature (**a**) nitrate (**c**), silicate (**e**) and phosphate (**g**). Section axis is shown in Fig. 1a. Left panels show the properties along an upstream shelf section including stations used as a reference for anomaly calculations. **b**,**d**,**f**,**h**, Isopycnal anomalies for **a**, **c**, **e** and **g**, respectively, with respect to the mean profile calculated from stations located upstream from Sermilik. Triangles in **a** and **b** show locations of hydrographic profiles. Circles in **b**–**h** correspond to discrete water sampling depths, while open triangles indicate additional sampling depths below the axis limit of the graph. Bathymetry is shown in all panels in dark grey, while black horizontal lines indicate the σ_θ (density) = 24.6, 26.6, 27.6 kg m^{-3} isopycnals.

shelf (Supplementary Fig. 6). Observational evidence for this export pathway along the Greenland margin is found in the temperature, salinity, nutrient and noble gas[32] signature of subsurface waters found 16 km downstream of the fjord mouth, which match the Sermilik Fjord GMW properties (Figs. 1b–d and 3 and Supplementary Fig. 7). This GMW layer appears between 130 and 150 m at the station closest to the coast, but not the offshore station, indicating that its horizontal extent is less than our coarse station spacing (4 km). The layer's small scale and isolation from the surface also suggest that complex turbulent processes mix the fjord waters into the East Greenland Coastal Current in the mouth region of Sermilik.

Resolving water mass composition

The significant enrichment of nitrate (Fig. 1d), a macronutrient present at low concentration (<2 μM) in ice and meltwater[10,41,42], suggests that the physical and biogeochemical properties of this modified water mass are largely set by entrained deep fjord waters. We trace the source of nutrient enrichment in the upper water column by quantitatively decomposing GMW into its water mass constituents using optimum multiparameter analysis (OMP)[43] (see Methods). We find that, owing to the large entrained AW content of glacially modified waters[32] (>85% of GMW by volume; Supplementary Fig. 8), and its high nutrient load, most of the dissolved macronutrients in GMW below the euphotic zone are sourced from upwelled ambient waters (contributing on average $NO_3^- > 96\%$, $Si(OH)_4 > 91\%$, $PO_4^{3-} > 95\%$ of the signal), as opposed to the injection of SGD and SMW from the GrIS. While previous observational data have suggested contributions from upwelling to nutrient enhancement along Arctic glacial margins[14,15,44–46], our study quantitatively demonstrates its dominance in a major glacial fjord by objectively parsing and comparing meltwater and ocean contributions to observed nutrient enrichment.

The consistency of anomaly maps, Θ–S_A–nutrient profiles, and OMP results with known fjord circulation and glacial meltwater

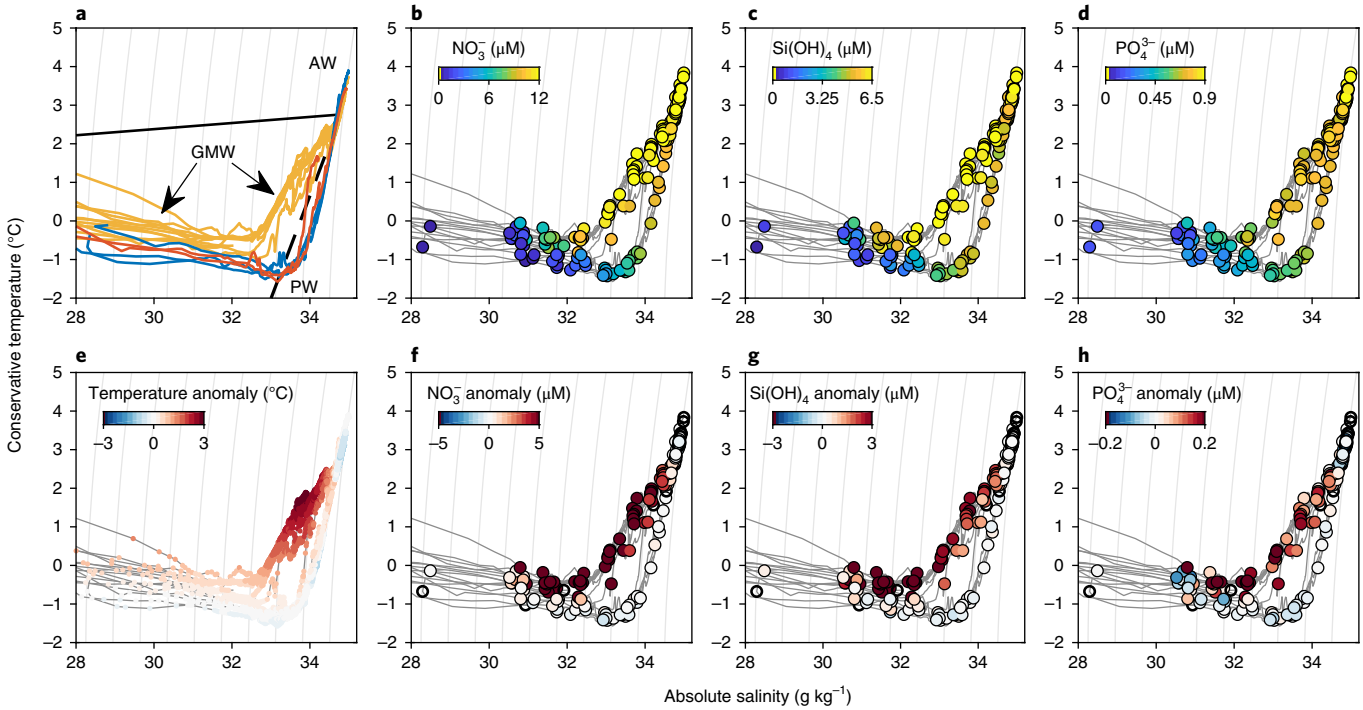

Fig. 3 | Evidence of subglacial discharge and submarine melt impacts on fjord waters. a, Θ–S_A plot showing water mass properties in Sermilik. Profiles are colour-coded according to Fig. 1a. Dominant water masses (AW, PW and GMW) are labelled in black, along with submarine meltwater (dashed black) and liquid runoff (solid black) mixing lines linking the oceanic AW endmember to SMW and SGD endmembers respectively (see Methods). **b**–**d**, Same as **a** with colours indicating concentrations of nitrate (**b**), silicate (**c**) and phosphate (**d**) for discrete water samples. **e**–**h**, Θ–S_A profiles are colour-coded with anomalies of conservative temperature (**e**), nitrate (**f**), silicate (**g**) and phosphate (**h**) (see Fig. 2). Light grey contours in all panels indicate isopcynals.

distributions[25,26,32,35,47] support our interpretation of GMW distribution and sources in this region. We conclude that the nutrient enrichment of GMW exported to the large-scale ocean from this major Greenland glacial fjord are largely set by the upwelling of deep water at the glacier margins, a previously neglected mechanism. Sermilik Fjord and Helheim Glacier share physical characteristics with a number of fjord systems along the GrIS margins[33,47,48], including Ilulissat Icefjord/Jakobshavn Isbræ (Greenland's largest glacial fjord system) where water mass characteristics and distributions similarly suggest that upwelled deep waters determine the nutrient enrichment of exported GMW (Supplementary Fig. 9). Based on these and previous field observations[14,15,24,25], we expect our conclusions to be broadly representative of other Greenland glacial fjords.

Nutrient exports from Greenland's glacial margins

Input of meltwater at glacier calving fronts drives a vertical transport of ambient waters whose volume is 10–30 times larger than the initial freshwater input[24,25,28,32]. For Sermilik Fjord, conservative estimates of seasonal (May–October) nutrient transports associated with the upwelling of AW average 17.1 ± 3.9 Gg yr^{-1} for nitrate (as N), 19.6 ± 4.5 Gg yr^{-1} for silicate (as Si) and 2.4 ± 0.5 Gg yr^{-1} for phosphate (as P; see Methods). Estimated transports for Ilulissat Icefjord are by comparison 2–3 times larger (40.1 ± 12.0 Gg yr^{-1} nitrate, 66.3 ± 19.9 Gg yr^{-1} silicate and 8.6 ± 2.6 Gg yr^{-1} phosphate) owing to the larger volume transport of runoff (SGD) into the fjord (Supplementary Fig. 10). These transports are substantial, in some cases equalling or exceeding nutrient exports by major rivers flowing into the Arctic (for example the Mackenzie River: 24 Gg yr^{-1} nitrate, 554 Gg yr^{-1} silica, 3 Gg yr^{-1} total dissolved phosphorus[49,50]; Table 1). Comparison of these ocean-sourced transports to total nutrients exported in meltwater from the GrIS (31 Gg N yr^{-1} total nitrogen[42], 280–4,480 Gg yr^{-1} silica[38] and 3.2 Gg yr^{-1} soluble reactive phosphorus[7]; Table 1) provides additional context. In the case of nitrate and phosphate, contributions of upwelled nutrients from one major glacial fjord alone rival that of the entire ice sheet, implying that for these nutrients, upwelling of deep ocean waters constitutes a dominant transport mechanism of nutrients to the surface ocean. Considering that phytoplankton in this region are primarily nitrate

Table 1 | Fjord nutrient transports

System	N (Gg yr^{-1})	P (Gg yr^{-1})	Si (Gg yr^{-1})	References
Sermilik Fjord (2015)	12.3	1.7	14.1	This study
Sermilik Fjord (2000–2016)	17.1 ± 3.9	2.4 ± 0.5	19.6 ± 4.5	This study
Ilulissat Icefjord (2000–-2016)	40.1 ± 12.0	8.6 ± 2.6	66.3 ± 19.9	This study
GrIS	31	3.2	280–4480	7,38,42
MacKenzie River	12.5–24	1–1.5	464–554	49,50,57
Yukon River	19–24	1.9–2	644–694	49,57,58
Yenisey River	8.7–29	5.4–14.3	200–1857	49,57

Comparison of Sermilik Fjord and Ilulissat Icefjord nutrient transports with published estimates for the GrIS as well as Arctic rivers draining the North American (MacKenzie and Yukon) and the Eurasian Arctic (Yenisey River, the largest in terms of discharge and nutrient fluxes[49,57]). All transports are reported as elemental (that is as N, P, Si) with units of Gg (10^9 g) yr^{-1}, and represent transports of dissolved nitrate, phosphate and silicate (fjords), total nitrogen, soluble reactive phosphorus, silica (GrIS), and nitrate, total dissolved phosphorus, and silica (rivers). Note that river export estimates are computed for the calendar year, while estimates for Sermilik and the GrIS reflect fluxes associated with or stemming from meltwater discharge, and therefore on average limited to the period between May and September. Averages and standard deviations are presented for both Sermilik and Ilulissat Icefjord, as well as transport estimates for Sermilik for the 2015 season individually.

and phosphate limited during summer months[51], this transport may have a disproportionately larger impact on regional primary production than meltwater nutrient export[14,15]. Conversely, depending on the particulate form of exported silica[38], glacial runoff may act as a comparatively larger source to the ocean (Table 1), although our combined transport estimate for Sermilik and Ilulissat still represents nearly 31% of the lower estimate for ice-sheet integrated meltwater silica export. In aggregate, our transport estimates suggest that Sermilik Fjord likely acts as a significant exporter of nutrients to the continental shelf. Because Southeast Greenland, one of the ice sheet's most prominent freshwater export pathways[29], is dominated by deep glacial fjords with marine-terminating glaciers exposed to AW[48], we hypothesize that the combined export of nutrient-rich GMW from these systems significantly contributes to regional primary production. Given the potential long-range transport of meltwater and GMW emanating from Southeast Greenland[11], this nutrient transport may ultimately have repercussions for carbon cycling farther downstream in the subpolar North Atlantic.

While the dominance of upwelling as a mechanism for nutrient enrichment is consistent for macronutrients, these conclusions may not hold for iron. Dissolved and particulate iron concentrations in meltwater emanating from the GrIS have been shown to reach micromolar concentrations (3–4 orders of magnitude higher than typical ocean concentrations)[8], implying that glacial exports could instead dominate upwelling transports in the case of this micronutrient. However, significant uncertainty remains concerning the fate of this iron in the marine environment[8,52], owing to its well-documented estuarine removal in coastal waters[53,54]. In Sermilik Fjord, we find TdFe enhancement in the fjord and downstream surface waters of 3–8 times the upstream concentration (Supplementary Fig. 3). Yet, these concentrations are 1–3 orders of magnitude lower than previously measured along coastal West Greenland[8,10], highlighting the high degree of spatial variability in iron concentrations along the GrIS margins resulting from differences in the source material, the chemical speciation of iron and its mode of export to the coastal ocean. A TdFe profile collected at the innermost fjord station provides further evidence of enhancement of iron in GMW, with TdFe concentrations below the euphotic zone strongly correlated with water column particulate load and a maximum TdFe concentration (12.8 ± 0.2 nM) at the core of the GMW plume (Supplementary Fig. 11). Concentrations in AW at depth are comparatively lower (3.0 ± 0.2 nM), values consistent with properties of subtropical source waters found offshore in the Irminger Basin[55]. This suggests that the GMW TdFe budget may, unlike other nutrients, be dominated by glacial iron transports. More detailed trace metal studies of fjords and adjacent glaciers are needed to constrain the importance of the GrIS for North Atlantic iron budgets and potential downstream effects on primary productivity[8,52].

Ecosystem response to glacially derived nutrient inputs ultimately depends not only on the characteristics and distribution of GMW (Figs. 1b–d and 2 and Supplementary Figs. 1 and 2), but also on the timing of its release to the continental shelf. Export was evident well below the euphotic zone outside the fjord in mid August 2015 (Fig. 1b–d and Supplementary Fig. 7), which, along with the Sermilik Fjord water mass distributions, suggests that a significant fraction of GMW nutrients may reach the continental shelf unmodified due to surface biological processes. The timescales over which these nutrient-rich waters are exported to the continental shelf is uncertain, though studies of the circulation in Sermilik Fjord suggest that timescales are on the order of weeks or months[34,35,47], in agreement with recent numerical model estimates[11]. As a result of the dynamic coupling between freshwater export and entrainment[22], our results suggest that an increase in glacial meltwater discharge from the GrIS over the coming decade, due to sustained warming of both atmosphere and ocean[18,29,56], is likely to enhance the export of nutrients from Greenland's glacial margins to the continental shelf and large-scale ocean, with repercussions for primary production. Several key uncertainties remain, however, including the role of iceberg-driven upwelling and meltwater release in biogeochemical cycling[21], a nutrient transport that may be out of phase with the seasonal cycle of meltwater release from the GrIS, as well as the bioavailability of particulate nutrients (that is P, Si, Fe), which constitute the largest solute exports from the ice sheet[6]. Coordinated observations across the atmosphere, ice sheet and ocean continuum[2], linked to more sophisticated ocean models, will be necessary to improve our understanding of the interactions between large-scale ocean dynamics, fjord circulation and the ice sheet, and determine the connection between GMW export and lower-trophic-level growth in the North Atlantic Ocean.

Online content

Any methods, additional references, Nature Research reporting summaries, source data, statements of data availability and associated accession codes are available at https://doi.org/10.1038/s41561-018-0268-4.

Received: 28 March 2018; Accepted: 4 November 2018;
Published online: 10 December 2018

References

1. Wadham, J. L. et al. The potential role of the Antarctic Ice Sheet in global biogeochemical cycles. *Earth Environ. Sci. Trans. R. Soc. Edinb.* **104**, 55–67 (2013).
2. O'Neel, S. et al. Icefield-to-ocean linkages across the northern Pacific coastal temperate rainforest ecosystem. *BioScience* **65**, 499–512 (2015).
3. Böning, C. W., Behrens, E., Biastoch, A., Getzlaff, K. & Bamber, J. L. Emerging impact of Greenland meltwater on deepwater formation in the North Atlantic Ocean. *Nat. Geosci.* **9**, 523–527 (2016).
4. Hodson, A. et al. Glacial ecosystems. *Ecol. Monogr.* **78**, 41–67 (2008).
5. Wadham, J. L. et al. Biogeochemical weathering under ice: size matters. *Global Biogeochem. Cycles* **24**, GB3025 (2010).
6. Hawkings, J. R. et al. The effect of warming climate on nutrient and solute export from the Greenland Ice Sheet. *Geochem. Perspect. Lett.* **1**, 94–104 (2015).
7. Hawkings, J. et al. The Greenland Ice Sheet as a hot spot of phosphorus weathering and export in the Arctic. *Global Biogeochem. Cycles* **30**, 191–210 (2016).
8. Bhatia, M. P. et al. Greenland meltwater as a significant and potentially bioavailable source of iron to the ocean. *Nat. Geosci.* **6**, 274–278 (2013).
9. Hawkings, J. R. et al. Ice sheets as a significant source of highly reactive nanoparticulate iron to the oceans. *Nat. Commun.* **5**, 3929 (2014).
10. Hopwood, M. J. et al. Seasonal changes in Fe along a glaciated Greenlandic fjord. *Front. Earth Sci.* **4**, 15 (2016).
11. Luo, H. et al. Oceanic transport of surface meltwater from the southern Greenland ice sheet. *Nat. Geosci.* **9**, 528–532 (2016).
12. Arrigo, K. R. et al. Melting glaciers stimulate large summer phytoplankton blooms in southwest Greenland waters. *Geophys. Res. Lett.* **44**, 6278–6285 (2017).
13. Oliver, H. et al. Exploring the potential impact of Greenland meltwater on stratification, photosynthetically active radiation, and primary production in the Labrador Sea. *J. Geophys. Res. Oceans* **123**, 2570–2591 (2018).
14. Meire, L. et al. Marine-terminating glaciers sustain high productivity in Greenland fjords. *Global Change Biol.* **23**, 5344–5357 (2017).
15. Kanna, N. et al. Upwelling of macronutrients and dissolved inorganic carbon by a subglacial freshwater driven plume in Bowdoin Fjord, Northwestern Greenland. *J. Geophys. Res. Biogeosci.* **123**, 1666–1682 (2018).
16. Enderlin, E. M. et al. An improved mass budget for the Greenland Ice Sheet. *Geophys. Res. Lett.* **41**, 866–872 (2014).
17. Straneo, F. & Cenedese, C. The dynamics of Greenland's glacial fjords and their role in climate. *Annu. Rev. Mar. Sci.* **7**, 89–112 (2015).
18. van den Broeke, M. et al. Partitioning recent Greenland mass loss. *Science* **326**, 984–986 (2009).
19. Rignot, E. & Mouginot, J. Ice flow in Greenland for the International Polar Year 2008–2009. *Geophys. Res. Lett.* **39**, L11501 (2012).
20. Chu, V. W. Greenland ice sheet hydrology: a review. *Prog. Phys. Geogr.* **38**, 19–54 (2014).
21. Moon, T. et al. Subsurface iceberg melt key to Greenland fjord freshwater budget. *Nat. Geosci.* **11**, 49–54 (2018).
22. Jenkins, A. Convection-driven melting near the grounding lines of ice shelves and tidewater glaciers. *J. Phys. Oceanogr.* **41**, 2279–2294 (2011).

23. Sciascia, R., Straneo, F., Cenedese, C. & Heimbach, P. Seasonal variability of submarine melt rate and circulation in an East Greenland fjord. *J. Geophys. Res. Oceans* **118**, 2492–2506 (2013).
24. Bendtsen, J., Mortensen, J., Lennert, K. & Rysgaard, S. Heat sources for glacial ice melt in a west Greenland tidewater outlet glacier fjord: the role of subglacial freshwater discharge. *Geophys. Res. Lett.* **42**, 4089–4095 (2015).
25. Beaird, N., Straneo, F. & Jenkins, W. Spreading of Greenland meltwaters in the ocean revealed by noble gases. *Geophys. Res. Lett.* **42**, 7705–7713 (2015).
26. Straneo, F. et al. Impact of fjord dynamics and glacial runoff on the circulation near Helheim Glacier. *Nat. Geosci.* **4**, 322–327 (2011).
27. Mortensen, J. et al. On the seasonal freshwater stratification in the proximity of fast-flowing tidewater outlet glaciers in a sub-Arctic sill fjord. *J. Geophys. Res. Oceans* **118**, 1382–1395 (2013).
28. Beaird, N., Straneo, F. & Jenkins, W. Characteristics of meltwater export from Jakobshavn Isbræ and Ilulissat Icefjord. *Ann. Glaciol.* **58**, 107–117 (2017).
29. Bamber, J., van den Broeke, M., Ettema, J., Lenaerts, J. & Rignot, E. Recent large increases in freshwater fluxes from Greenland into the North Atlantic. *Geophys. Res. Lett.* **39**, L19501 (2012).
30. Harden, B. E., Straneo, F. & Sutherland, D. A. Moored observations of synoptic and seasonal variability in the East Greenland Coastal Current. *J. Geophys. Res. Oceans* **119**, 8838–8857 (2014).
31. Sutherland, D. A., Straneo, F. & Pickart, R. S. Characteristics and dynamics of two major Greenland glacial fjords. *J. Geophys. Res. Oceans* **119**, 3767–3791 (2014).
32. Beaird, N. L., Straneo, F. & Jenkins, W. Export of strongly diluted Greenland meltwater from a major glacial fjord. *Geophys. Res. Lett.* **45**, 4163–4170 (2018).
33. Straneo, F. et al. Rapid circulation of warm subtropical waters in a major glacial fjord in East Greenland. *Nat. Geosci.* **3**, 182–186 (2010).
34. Straneo, F. et al. Characteristics of ocean waters reaching Greenland's glaciers. *Ann. Glaciol.* **53**, 202–210 (2012).
35. Jackson, R. H. & Straneo, F. Heat, salt, and freshwater budgets for a glacial fjord in Greenland. *J. Phys. Oceanogr.* **46**, 2735–2768 (2016).
36. Lydersen, C. et al. The importance of tidewater glaciers for marine mammals and seabirds in Svalbard, Norway. *J. Mar. Syst.* **129**, 452–471 (2014).
37. Azetsu-Scott, K. & Syvitski, J. P. M. Influence of melting icebergs on distribution, characteristics and transport of marine particles in an East Greenland fjord. *J. Geophys. Res. Solid Earth* **104**, 5321–5328 (1999).
38. Hawkings, J. R. et al. Ice sheets as a missing source of silica to the polar oceans. *Nat. Commun.* **8**, 14198 (2017).
39. Gade, H. G. Melting of ice in sea water: a primitive model with application to the Antarctic Ice Shelf and icebergs. *J. Phys. Oceanogr.* **9**, 189–198 (1979).
40. Jenkins, A. The impact of melting ice on ocean waters. *J. Phys. Oceanogr.* **29**, 2370–2381 (1999).
41. Bhatia, M. P. *Hydrological and Biogeochemical Cycling along the Greenland Ice Sheet Margin*. PhD thesis, Massachusetts Institute of Technology (2012).
42. Wadham, J. L. et al. Sources, cycling and export of nitrogen on the Greenland Ice Sheet. *Biogeosciences* **13**, 6339–6352 (2016).
43. Tomczak, M. & Large, D. G. B. Optimum multiparameter analysis of mixing in the thermocline of the eastern Indian Ocean. *J. Geophys. Res. Oceans* **94**, 16141–16149 (1989).
44. Hartley, C. H. & Dunbar, M. J. On the hydrographic mechanism of the so-called brown zones associated with tidal glaciers. *J. Mar. Res.* **1**, 305–311 (1938).
45. Dunbar, M. J. Glaciers and nutrients in Arctic fiords. *Science* **182**, 398–398 (1973).
46. Horne, E. P. W. Ice-induced vertical circulation in an Arctic fiord. *J. Geophys. Res.* **90**, 1078–1086 (1985).
47. Jackson, R. H., Straneo, F. & Sutherland, D. A. Externally forced fluctuations in ocean temperature at Greenland glaciers in non-summer months. *Nat. Geosci.* **7**, 503–508 (2014).
48. Millan, R. et al. Vulnerability of Southeast Greenland glaciers to warm Atlantic water from Operation IceBridge and Ocean Melting Greenland data. *Geophys. Res. Lett.* **45**, 2688–2696 (2018).
49. Holmes, R. M. et al. Seasonal and annual fluxes of nutrients and organic matter from large rivers to the Arctic Ocean and surrounding seas. *Estuaries Coast.* **35**, 369–382 (2011).
50. Emmerton, C. A., Lesack, L. F. W. & Vincent, W. F. Nutrient and organic matter patterns across the Mackenzie River, estuary and shelf during the seasonal recession of sea-ice. *J. Mar. Syst.* **74**, 741–755 (2008).
51. Meire, L. et al. High export of dissolved silica from the Greenland Ice Sheet. *Geophys. Res. Lett.* **43**, 9173–9182 (2016).
52. Hopwood, M. J., Bacon, S., Arendt, K., Connelly, D. P. & Statham, P. J. Glacial meltwater from Greenland is not likely to be an important source of Fe to the North Atlantic. *Biogeochemistry* **124**, 1–11 (2015).
53. Boyle, E. A., Edmond, J. M. & Sholkovitz, E. R. The mechanism of iron removal in estuaries. *Geochim. Cosmochim. Acta* **41**, 1313–1324 (1977).
54. Schroth, A. W., Crusius, J., Hoyer, I. & Campbell, R. Estuarine removal of glacial iron and implications for iron fluxes to the ocean. *Geophys. Res. Lett.* **41**, 3951–3958 (2014).
55. Achterberg, E. P. et al. Iron biogeochemistry in the high latitude North Atlantic Ocean. *Sci. Rep.* **8**, 1283 (2018).
56. Straneo, F. & Heimbach, P. North Atlantic warming and the retreat of Greenland's outlet glaciers. *Nature* **504**, 36–43 (2013).
57. Fouest, V. L., Babin, M. & Tremblay, J. É. The fate of riverine nutrients on Arctic shelves. *Biogeosciences* **10**, 3661–3677 (2013).
58. Guo, L., Zhang, J.-Z. & Guéguen, C. Speciation and fluxes of nutrients (N, P, Si) from the upper Yukon River. *Global Biogeochem. Cycles* **18**, GB1038 (2004).

Acknowledgements

This work was supported by: an internal grant from the Woods Hole Oceanographic Institution (WHOI) Ocean and Climate Change Institute (to M.R.C., F.S. and M.A.C.), grants from the National Science Foundation to M.A.C. (OCE-1458305), N.B. (OCE-1536856) and F.S. (OCE-1657601), and Woods Hole Oceanographic Institution Postdoctoral Fellowships to M.R.C. and R.M.B. We are grateful to J. Hawkings for sharing Leverett Glacier nutrient data, to K. Azetsu-Scott and B. Curry for sharing the Davis Strait and West Greenland continental shelf hydrographic data, to P. Henderson and the WHOI Nutrient Analytical Facility for assistance with macronutrient sample collection and analysis, to R. Jackson for helpful conversations concerning data analysis, to A. Ramsey for logistical support, to S. Laney for loan of and technical assistance with oceanographic instrumentation, to M. Swartz for CTD assembly and testing, and to the captain and crew of the RV *Adolf Jensen* for support in the field.

Author contributions

M.R.C. and F.S. conceived the study with input from M.A.C. M.R.C., F.S. and N.B. collected data and samples in the field. M.A.C. and R.M.B analysed water samples. M.R.C., N.B. and R.M.B. analysed the resulting data. M.R.C. wrote the paper, with assistance from all co-authors.

Competing interests

The authors declare no competing interests.

Additional information

Supplementary information is available for this paper at https://doi.org/10.1038/s41561-018-0268-4.

Reprints and permissions information is available at www.nature.com/reprints.

Correspondence and requests for materials should be addressed to M.R.C.

Publisher's note: Springer Nature remains neutral with regard to jurisdictional claims in published maps and institutional affiliations.

Methods

Field sampling. Samples and observations were collected from 3 to 11 August 2015 aboard the RV *Adolf Jensen*. Conductivity, temperature and depth (CTD) profiles between the surface and 10 m above bottom were collected using a SBE 25plus Sealogger CTD (Sea-Bird Scientific) equipped with a Wetlabs ECO-Triplet (chlorophyll *a*, chromophoric dissolved organic matter and backscattering at 700 nm), a Satlantic PAR LOG 7000 m photosynthetically available radiation sensor, and a SBE 43 dissolved oxygen sensor. We report temperature and salinity as conservative temperature (Θ) and absolute salinity (S_A), respectively (http://www.teos-10.org).

Macronutrient sampling and analysis. Nutrient samples for quantification of nitrate + nitrite, phosphate and silicate were collected using twelve 5 l Niskin bottles (Ocean Test Equipment) equipped with silicone o-rings and coated springs, mounted on a Sea-Bird rosette and deployed from the ship using a Spectra line (Honeywell). Samples were filtered through a sterile 0.22 µM Sterivex filter and kept frozen at −20 °C for later analysis at the Woods Hole Oceanographic Institution Nutrient Analytical Facility. To allow for sufficient time for any silicate polymers formed during storage to return to their reactive form, samples were thawed in the dark at room temperature for 24 h (ref. [59]). Dissolved nutrient concentrations were quantified using a SEAL AA3 four-channel segmented flow analyser[60] using standard colorimetric methods[61] for nitrate + nitrite (NOx G172-96), phosphate (G-297-03) and silicate (G177-96). All samples were measured in duplicate with precision for reported values of 0.7%, 6.8% and 1.4% for nitrate + nitrite, phosphate and silicate, respectively. Measurement accuracy was determined via analysis of the KANSO reference material for nutrients in seawater (RMNS) certified standard RMIJ CRM 7602A. The measured/certified values for nitrate + nitrite, phosphate and silicate were 1.004, 1.008 and 0.970, respectively.

Iron sampling and analysis. All bottles and plasticware were cleaned using trace metal clean procedures outlined in the US GEOTRACES protocols[62]. Surface samples for TdFe were collected using a trace metal clean sampler fixed to a plastic pole. Samples were taken while the ship was steaming at approximately 1 knot to minimize contamination from the ship. Water column samples were also opportunistically collected at the innermost fjord station using the Niskin bottles mounted to the rosette (Supplementary Fig. 11). Unfiltered samples were placed in separate trace metal clean 250 ml low-density polyethylene bottles and immediately acidified to pH 1.8 with 4 ml l^{-1} Optima HCl (Fisher Scientific) and stored until analysis 4 months later in the lab at the Woods Hole Oceanographic Institution. TdFe is operationally defined as comprising the total dissolved Fe and labile particulate Fe[63], and likely represents the most reactive, and perhaps the most bioavailable, portion of the total Fe pool.

Analyses for TdFe were carried out by first filtering each sample with a clean 0.2 µm polycarbonate filter. The filtered samples were then slowly neutralized to pH 8 with 1 N Optima NH_4OH (Fisher Scientific) and ultraviolet-oxidized for 1 hour in acid-cleaned quartz tubes using a temperature controlled UV Digester 909 (Metrohm). Then 50 µl of 1.5 M ammonium borate buffer (>99.99% boric acid, Alfa Aesar; 0.4 N optima ammonium hydroxide Fisher Scientific) was added to each 10 ml sample aliquot (pH 8.2, NBS scale) along with 5 µM salicylaldoxime (Acros Organics, VWR) and left to equilibrate overnight. Samples were subsequently measured in triplicate using standard addition methods and cathodic stripping voltammetry on an Eco-Chemie µ Autolab III coupled to a 663 VA stand (Metrohm) and processed using NOVA 8.0 software. Instrument parameters were set following a previous study[64].

Disko Bay observations. Hydrographic observations from Disko Bay were obtained from the World Ocean Database at the National Oceanographic Data Center (https://www.nodc.noaa.gov; cruise WOD13_DK001270) and the International Council for the Exploration of the Sea (ICES) oceanographic database (http://ocean.ices.dk; cruise 26AJ). These data are available as a supplementary dataset, as well as via the aforementioned public databases. Samples flagged as being of questionable or poor quality were omitted in this analysis.

Water mass properties. Physical and biogeochemical properties of distinct water masses (that is AW, PW, Warm Polar Water) or of portions of the water column (for example fjord waters between 30 and 250 m) are unless otherwise indicated presented as mean ± standard deviation.

Water mass analysis. OMP is a common water mass analysis technique that uses known physical and chemical properties of water-type endmembers (that is, source waters) to solve for their fractional contributions to a mixture (that is, a particular water sample) assuming linear mixing[43]. Here we use OMP as employed by ref. [25] to quantify the composition of GMW along Sermilik Fjord. Formally this technique amounts to solving a system of m linear mixing equations for each of m observed tracers:

$$\sum_{i=1}^{n} f_i A_{ij} = d_{\mathrm{obs},j} \tag{1}$$

where n denotes the number of source waters, f_i the fraction of the ith source water in the mixture, A_{ij} the tracer value (for example temperature) for the particular source water, and $d_{obs,j}$ the jth observed water sample. An additional constraint is placed so that the sum of fractions equals to one (that is a mass balance constraint). This system of equations can be written as:

$$\mathbf{Ax}-\mathbf{d}=\mathbf{r} \tag{2}$$

where $\mathbf{A}$ is the $(m+1)\times n$ matrix of the source-water tracer values (with the entries in the last row set to 1 to denote the mass balance constraint), $\mathbf{x}$ is the $n\times 1$ vector of unknown fractions of source water in the mixture, $\mathbf{d}$ is a $(m+1)\times 1$ vector of the observed tracers in a sample, and $\mathbf{r}$ is the $(m+1)\times 1$ residual misfit between the observed tracers and the combination of endmembers. This system of equations is solved as a least squares problem (for example, minimizing $\|\mathbf{r}\|$) subject to the requirement that there be as many or more constraining tracer equations than unknown water-type fractions (that is $m \geq n$) and the constraint that the resulting water mass fractions be non-negative[43].

We define endmember properties (that is $\mathbf{A}$), whose values appear in Supplementary Table 1, following the method of ref. [25]. For oceanic sources, we examine temperature/salinity properties of upstream waters (the proximal source waters for Sermilik Fjord), defining temperature and salinity endmember values of three water masses—AW, PW and Warm Polar Water—based on particular Θ–S_A signatures identified in previous surveys[26,31,35,47] (Fig. 3a). Source-water nutrient concentrations are then defined by the properties of the water sample closest in thermohaline space to the Θ–S_A definition of that water mass (Fig. 3b–d). Following previous studies[65,66], and because this analysis is both limited to the scale of the fjord (<100 km) and focuses on properties of waters below the euphotic zone (approximately 30 m), we treat macronutrients, alongside Θ and S_A, as conservative tracers, ignoring biogeochemical modifications resulting from water mass aging or primary production.

Properties for the two glacial source waters, SGD and SMW, are assigned based on literature values. SGD, formed as a result of melting at the surface of the ice sheet, is assumed to enter the fjord with a temperature of approximately 0 °C. SMW, formed as a result of ocean melting at depth, requires latent heat to be drawn from the ocean during phase change[39,40]. In the framework of OMP, this yields an effective tracer temperature of −87 °C (ref. [25]). Both water masses are assumed to have 0 salinity. Glacial nutrient concentrations, which were not measured during our survey, are estimated by averaging recent observations collected from a range of West Greenland glacier–fjord systems for nitrate[41,42], silicate[6,38,41] and phosphate[6,7,41].

Before solving equation (2), $\mathbf{A}$ and $\mathbf{d}$ are first normalized (subtracting the mean and dividing by the standard deviation) to make parameters of different units and magnitudes comparable, and then weighted to account for measurement accuracy, our knowledge of true endmember properties and the spread of property values[43]. Weighing ultimately reflects differences in the tracers' abilities to distinguish between water masses for a given observed water sample. Weights for each tracer in matrix $\mathbf{A}$ are computed as:

$$W_j = \frac{\sigma_j^2}{\varepsilon_{j,\max}^2} \tag{3}$$

where σ_j^2 refers to the variance of the endmember tracer values $\left(\sigma_j^2 = \frac{1}{n}\sum_{i=1}^{n}(A_{ij}-A_j)^2\right)$ and $\varepsilon_{j,\max}$ denotes the largest uncertainty in that tracer parameter across all endmembers. Values of $\varepsilon_{j,\max}$ used in this study appear in parentheses in Supplementary Table 1. Large uncertainties are associated with glacial source-water nutrient concentrations, given difficulties associated with measuring SMW directly in glacial fjords and the large spatial and temporal variability in observed values for SGD within and across sampling sites[6,7,38,41,42]. Uncertainties for temperature and salinity are set to match those of ref. [25], given similarities in physical systems and sampling methods. Following previous studies[43], we assigned the largest of our calculated weights to the mass balance equation.

In our case, equation (2) was thus modified to include a $(m+1)\times(m+1)$ diagonal weighing matrix $\mathbf{W}$, whose entries W_{ij} are given by equation (3), and the system solved by minimizing the norm of the residual ($\|\mathbf{r}\|^2$):

$$(\mathbf{Ax}-\mathbf{d})^{\mathrm{T}}\mathbf{W}^{\mathrm{T}}\mathbf{W}(\mathbf{Ax}-\mathbf{d}) = \mathbf{r}^{\mathrm{T}}\mathbf{r} \tag{4}$$

where $^{\mathrm{T}}$ denotes matrix transpose. Following ref. [43] and others, we use water mass conservation residuals as an indicator for the quality of the OMP results. Low (high) water mass conservation residuals, typically <5%, suggest that observations can be well (poorly) described as a combination of the specified source-water types. We also compare OMP results computed as above to results from an independent analysis of Sermilik water masses employing noble gases as tracers[32] (Supplementary Fig. 8). Data output from this analysis were obtained from the authors.

GMW nutrient budget. Fractional water mass contributions derived from OMP (Supplementary Fig. 8) combined with endmember nutrient concentrations (Supplementary Table 1) allow us to apportion water column nutrients to glacial

and oceanic water masses[67]. For fjord waters where glacial contributions were identified in OMP (that is SMW or SGD > 0), percent contributions to each macronutrient load for each discrete sampling location (F_i) was calculated as:

$$F_i = \frac{f_i A_{ij}}{d_{\mathrm{obs},j}} \quad (5)$$

with f_i, A_{ij} and $d_{\mathrm{obs},j}$ as in equation (1). Nutrient budgets quoted in the text represent the mean fractional contribution of each water mass to total nutrient concentrations for GMW across the fjord.

Transports. Export of nutrients in the upper layer of the fjord at the time of sampling was calculated by multiplying the along-fjord geostrophic velocity section[32] with the nutrient distributions (Supplementary Fig. 6), then integrating across the fjord (black section in Fig. 1a) and from the surface to the bottom of the GMW layer (approximately above the 34.5 isohaline).

To derive annual estimates of vertical nutrient transports resulting from ice–ocean interactions, we assume that upwelling is to a first order driven by the input of subglacial discharge at the base of the glacier[25,28,68]. We use daily estimates of runoff at 1 km resolution derived from downscaled Regional Atmospheric Climate Model (RACMO) v2.3.2[69] to estimate the SGD volume flux into Sermilik at the margin of Helheim Glacier and into Ilulissat Icefjord at the margin of Jakobshavn Isbræ between 1959 and 2016 (Supplementary Fig. 10). Catchment basin definitions were obtained from ref. [70] for Helheim and the National Snow and Ice Data Center for Jakobshavn (http://nsidc.org/data/nsidc-0371)[71,72]. In estimating the volume flux of SGD at the base of Helheim, we assume that surface runoff for a particular day is immediately transferred to the bed and exported to the fjord at the glacier base, implying that runoff is stored neither in the firn nor at the ice-sheet bed.

For Sermilik, we use a median entrainment ratio of $\frac{f_{\mathrm{AW}}}{f_{\mathrm{SGD}}} = \frac{30}{1}$ for GMW in the top 250 m, a value derived from OMP results that is consistent with ambient to meltwater entrainment ratios previously observed in two West Greenland fjords[25,28] as well as an independent estimate for Sermilik Fjord[32], and calculate the volume flux of AW into the upper water column by multiplying the SGD time series by 30. For Ilulissat Icefjord, where both AW and PW comprise significant components of GMW, we used entrainment ratios of 14 and 16 respectively, median values for the upper water column derived from a previous noble gas-based OMP analysis of GMW water mass composition[28] (Supplementary Fig. 9).

Dissolved nutrient transports for each year (that is, period between approximately May and September of each year for which RACMO runoff for each catchment basin is >0) are calculated from the product of the integrated oceanic volume flux (either AW or AW + PW) and the endmember nutrient concentrations (Supplementary Tables 1 and 2). Nutrient endmember concentrations for source-water masses to Disko Bay most similar (in temperature–salinity space) to water masses encountered during sampling in ref. [28] were obtained from an average of properties of upstream source waters to the bay[73] (Supplementary Fig. 12 and Supplementary Table 2). Averages fluxes and standard deviations for the 2000–2016 period, as well as nutrient fluxes for 2015 for Sermilik individually, are reported in the text and in Table 1.

Our approach for calculating nutrient transport uses a simplified model that relies on the availability of time series runoff estimates. Because it ignores the contribution of upwelling due to submarine melt (thought to be at least as large as the volume flux of subglacial discharge in Sermilik[32,35]), for which long-term estimates are unavailable, our volume fluxes of AW (here computed as 30 times SGD) are necessarily underestimated. Uncertainty estimates for daily RACMO runoff are unavailable as part of model output[69], although previous model intercomparisons yield estimates on the order of 20% for the GrIS[74,75], with uncertainties varying regionally. While runoff fluxes derived from RACMO for both Helheim and Jakobshavn are overall similar to previous estimates reported in the literature from another regional model[70,76], estimates for our occupation of Sermilik ($265 \pm 126\ \mathrm{m^3\,s^{-1}}$, Supplementary Fig. 13) are 2–4 times lower than those calculated from in situ measurements of water mass distributions and geostrophic velocities for the same time period ($800 \pm 500\ \mathrm{m^3\,s^{-1}}$; ref. [32]). This discrepancy can be accounted for by an underestimation of model runoff exported at the base of Helheim, or by considering that we ignore the impact of subglacial discharge from the smaller but also deeply grounded Midgaard and Fenris glaciers (Fig. 1a), whose combined catchment-scale subglacial fluxes into Sermilik (peaking seasonally at approximately $1{,}000\ \mathrm{m^3\,s^{-1}}$; ref. [21]) rival those of Helheim. Accounting for these additional deep sources of freshwater would yield concomitant increases in the volume of entrained ocean waters[17,22,68], thereby significantly increasing nutrient transport estimates.

Data availability

Continuous hydrographic (CTD) profiles are available from the National Oceanographic Data Center (http://accession.nodc.noaa.gov/0171277), while discrete nutrient measurements and CTD bottle data (https://doi.org/10.1594/PANGAEA.887304), as well as discrete iron data (https://doi.org/10.1594/PANGAEA.887324), are available from the PANGEA information system[77,78]. Ocean current data for Sermilik Fjord are publicly available from Data.gov(NODC accession number 0126772 and NCEI accession number 0127325). Downscaled RACMO2.3.2 data were provided by M. van den Broeke and B. Noël and are available from them upon request. Hydrographic data for the West Greenland continental shelf (Supplementary Table 2 and Supplementary Fig. 12) are available from K. Azetsu-Scott upon request. Other data supporting the findings of this study are available as described in the Methods, and otherwise from the corresponding author upon request.

References

59. Macdonald, R. W., McLaughlin, F. A. & Wong, C. S. The storage of reactive silicate samples by freezing. *Limnol. Oceanogr.* **31**, 1139–1142 (2003).
60. Rice, E. W., Baird, R. B., Eaton, A. D. & Clesceri, L. S. (eds) *Standard Methods for the Examination of Water and Wastewater* 22nd edn (American Public Health Association, American Water Works Association (AWWA), Water Environment Federation, Washington DC, 2012).
61. Grasshoff, K., Kremling, K. & Ehrhardt, M. (eds) *Methods of Seawater Analysis* 3rd edn (Wiley-VCH Verlag, Weinheim, 2007).
62. Cutter, G. A. Intercalibration in chemical oceanography—getting the right number. *Limnol. Oceanogr. Methods* **11**, 418–424 (2013).
63. Martin, J. H. et al. Testing the iron hypothesis in ecosystems of the equatorial Pacific Ocean. *Nature* **371**, 123–129 (1994).
64. Abualhaija, M. M. & van den Berg, C. M. G. Chemical speciation of iron in seawater using catalytic cathodic stripping voltammetry with ligand competition against salicylaldoxime. *Mar. Chem.* **164**, 60–74 (2014).
65. Hinrichsen, H. H. & Tomczak, M. Optimum multiparameter analysis of the water mass structure in the western North Atlantic Ocean. *J. Geophys. Res. Oceans* **98**, 10155–10169 (1993).
66. Karstensen, J. & Tomczak, M. Age determination of mixed water masses using CFC and oxygen data. *J. Geophys. Res. Oceans* **103**, 18599–18609 (1998).
67. Saito, M. A. et al. Slow-spreading submarine ridges in the South Atlantic as a significant oceanic iron source. *Nat. Geosci.* **6**, 775–779 (2013).
68. Carroll, D. et al. Modeling turbulent subglacial meltwater plumes: implications for fjord-scale buoyancy-driven circulation. *J. Phys. Oceanogr.* **45**, 2169–2185 (2015).
69. Noël, B. et al. A daily, 1 km resolution data set of downscaled greenland ice sheet surface mass balance (1958–2015). *Cryosphere* **10**, 2361–2377 (2016).
70. Mernild, S. H. et al. Freshwater flux to Sermilik Fjord, SE Greenland. *Cryosphere* **4**, 453–465 (2010).
71. Lewis, S. *Hydrologic Sub-basins of Greenland* Version 1 (National Snow and Ice Data Center, Boulder, 2009).
72. Lewis, S. M. & Smith, L. C. Hydrologic drainage of the Greenland Ice Sheet. *Hydrol. Process.* **23**, 2004–2011 (2009).
73. Azetsu-Scott, K., Petrie, B., Yeats, P. & Lee, C. Composition and fluxes of freshwater through Davis Strait using multiple chemical tracers. *J. Geophys. Res. Oceans* **117**, C12011 (2012).
74. Vernon, C. L. et al. Surface mass balance model intercomparison for the Greenland Ice Sheet. *Cryosphere* **7**, 599–614 (2013).
75. Sutterley, T. C. et al. Evaluation of reconstructions of snow/ice melt in Greenland by regional atmospheric climate models using laser altimetry data. *Geophys. Res. Lett.* **45**, 8324–8333 (2018).
76. Mernild, S. H. et al. Freshwater flux and spatiotemporal simulated runoff variability into Ilulissat Icefjord, West Greenland, linked to salinity and temperature observations near tidewater glacier margins obtained using instrumented ringed seals. *J. Phys. Oceanogr.* **45**, 1426–1445 (2015).
77. Cape, M. R., Straneo, F. & Charette, M. A. Hydrographic sensor and bottle data collected during an August 2015 cruise to Sermilik Fjord, East Greenland. *PANGAEA* https://doi.org/10.1594/PANGAEA.887304(2018).
78. Cape, M. R., Bundy, R. M. & Straneo, F. Surface total dissolvable iron data collected during an August 2015 cruise to Sermilik Fjord, East Greenland. *PANGAEA* https://doi.org/10.1594/PANGAEA.887324(2018).